Received: 18 December 2019 | Revised: 8 May 2020 | Accepted: 20 May 2020

DOI: 10.1002/nme.6444

RESEARCH ARTICLE

WILEY

An improved immersed moving boundary for hydrodynamic force calculation in lattice Boltzmann method

Zhiqiang Chen | **Moran Wang**

Department of Engineering Mechanics and CNMM, Tsinghua University, Beijing, China

Correspondence
Moran Wang, Department of Engineering Mechanics and CNMM, Tsinghua University, Beijing 100084, China.
Email: mrwang@tsinghua.edu.cn

Funding information
National Science Foundation of China, Grant/Award Number: 11761131012, U1837602; National Science and Technology Major Project on Oil and Gas, Grant/Award Number: 2017ZX05013001; Tsinghua University Initiative Scientific Research Program

Summary

Particles suspension is considerably prevalent in petroleum industry and chemical engineering. The efficient and accurate simulation of such a process is always a challenge for both the traditional computational fluid dynamics and lattice Boltzmann method. Immersed moving boundary (IMB) method is promising to resolve this issue by introducing a particle-fluid interaction term in the standard lattice Boltzmann equation, which allows for the smooth hydrodynamic force calculation even for a large grid size relative to the solid particle. Although the IMB method was proved good for stationary particles, the deviation of hydrodynamic force on moving particles exists. In this work, we reveal the physical origin of this problem first and figure out that the internal fluid effect on the hydrodynamic force calculation is not counted in the previous IMB. An improved immersed moving boundary method is therefore proposed by considering the internal fluid correction, which is easy to implement with the little extra computation cost. A 2D single elliptical particle and a 3D sphere sedimentation in Newtonian fluid is simulated directly for the validation of the corrected model by excellent agreements with the standard data.

KEYWORDS

fluid-particle interaction, immersed moving boundary, internal fluid effect, lattice Boltzmann method, particles suspension

1 | INTRODUCTION

The efficient and accurate simulation of particles suspension is of both academic and industrial interests such as fluidized beds in the chemical engineering and sand production or hydraulic fracture in the petroleum industry.[1-7] In order to gain fundamental insights into these poorly understood problems, a direct numerical simulation (DNS) is needed where the Navier-Stokes equations for an incompressible Newtonian fluid is solved directly or equivalently and the particle-fluid interaction should be considered at the particle scale.[8,9] Recently, the lattice Boltzmann method (LBM) has been a powerful tool to directly couple a large number of moving particles and the fluid.[10,11]

A moving boundary condition and the accurate calculation of hydrodynamic force imposed on the solid particle are two basic aspects in LBM simulation of particles suspension.[11] Early models to consider particles suspension are based on the momentum exchange such as the shell model[1,2] and the dry particle model,[12,13] where particle representation is stepwise, which results in the hydrodynamic force fluctuation when the particle covers or uncovers the LBM cells.[11,14] To reduce the hydrodynamic force fluctuation a modified momentum exchange method is proposed by considering the

initial momentum of the net mass transfer at each time step.[11] Some other methods to achieve a smoother hydrodynamic force calculation include the interpolation-based curved boundary models[15,16] and the stress integration models.[17,18] However, although some efforts have been made during the past few decades, it is still a challenge to achieve a smooth and accurate calculation of hydrodynamic force without increasing the resolution of the computation domain in the particles suspension models.[9]

This article focuses on the immersed moving boundary (IMB) method proposed in Reference [19] and later extended by Reference [8, 9]. It offers particle representation at a subcell scale and allows for smooth hydrodynamic force calculation even for a large LBM cell size relative to the solid particle.[8,9,19,20] According to the result in Reference [11], forces on the particle obtained by IMB are the smoothest among all the method they tested. During the past few decades, this model has been widely applied to explore the underlying physics of dense particles suspension,[14,21-30] where thousands of particles immersed in the fluid were considered. IMB method was validated in the previous work by simulating the fluid flow through a fixed particle,[9] and the calculated drag coefficient agreed well with other numerical and empirical results. However, the error exists in IMB method for the dynamic cases. Chen et al[11] simulated the settling process of a single elliptical particle by different lattice Boltzmann-based methods, and they found the particle trajectories obtained by IMB method deviate from FEM results when the particle Reynolds number (Re) is relatively high.

Although IMB method gives a sufficiently smooth hydrodynamic force and is proved accurate for the still particles, it results in the inaccurate particle dynamics. Thus, the purpose of this work is to answer the question why IMB method cannot give accurate hydrodynamic force in the dynamic cases, and then an improved IMB method is proposed based on the strict mathematic derivation of the hydrodynamic force. The rest of this article is organized as follows. First the original IMB method is briefly introduced in Section 2. In Section 3, an improved IMB method is proposed including the mathematic derivation of the hydrodynamic force. Section 4 is the validation of the new model, where the comparisons between the original IMB method and the improved one are presented. In the last section, the article is concluded.

2 | ORIGINAL IMMERSED MOVING BOUNDARY METHOD FOR LBM

Generally, the immersed boundary methods (IBM)[31-36] is a group of numerical techniques to consider the coupling between the fluid flow and the solid movement.[37] Here, we focus on immersed moving boundary (IMB) for LBM which is different from the traditional immersed boundary method (IBM). It is proposed in Reference [19] and then extended in.[8-10] In the following parts, the lattice Boltzmann method (LBM) and the IMB method are briefly introduced, respectively.

2.1 | Lattice Boltzmann method (LBM)

Lattice Boltzmann method (LBM) is an efficient numerical method for solving the partial differential equations especially with complicated boundary condition such as porous media and particle suspensions.[38-44] Different from the traditional computational fluid dynamics (CFD), where the macroscopic governing equations (such as Navier-Stokes equations) are solved directly, LBM solves Boltzmann equation in the finite discrete velocities space, while according to the Chapman-Enskog expansion the Navier-Stokes equations can be recovered.[45] Thus, the basic variables in LBM is the particle distribution function, f_i. In the lattice Bhatnagar-Cross-Krook model, the particle distribution is governed by the evolution equation written as[45]

$$f_i(\boldsymbol{x}+\boldsymbol{e_i}\delta_t, t+\delta_t) = f_i(\boldsymbol{x}, t) - \frac{1}{\tau}(f_i(\boldsymbol{x}, t) - f_i^{\mathrm{eq}}(\rho, \boldsymbol{u})) + \boldsymbol{F_i}\delta_t, \qquad i = 0\text{-}9, \tag{1}$$

where $\boldsymbol{x}$ denotes the position vector, f_i is the particle distribution function in the ith lattice discrete velocity direction $\boldsymbol{e_i}$, f_i^{eq} is the corresponding equilibrium distribution, δ_t is the time step, $\boldsymbol{F_i}$ is the discrete external force in direction $\boldsymbol{e_i}$, and τ is the dimensionless relaxation time related to the kinematic viscosity

$$\nu = \frac{(\tau - 0.5)\delta_x^2}{3\delta_t}, \tag{2}$$

where δ_x is the lattice size.

In this work, both 2D and 3D cases are considered. The algorithm details can be found in our previous publications[11,22,46,47] or other books.[48] For an example of the D2Q9 model, the discrete velocities are

$$e_i = \begin{cases} 0, & i = 0 \\ c(\cos[(i-1)\pi/4], \sin[(i-1)\pi/4]), & i = 1,3,5,7 \\ c(\sqrt{2}\cos[(i-1)\pi/4], \sqrt{2}\sin[(i-1)\pi/4]), & i = 2,4,6,8 \end{cases}, \tag{3}$$

where $c = \delta_x/\delta_t$. The equilibrium distribution for D2Q9 is given as

$$f_i^{\mathrm{eq}}(\rho, \boldsymbol{u}) = \rho w_i \left[1 + \frac{e_i \cdot \boldsymbol{u}}{3c^2} + \frac{9(e_i \cdot \boldsymbol{u})^2}{2c^4} - \frac{3\boldsymbol{u} \cdot \boldsymbol{u}}{2c^2}\right], \tag{4}$$

where the weighting factors are

$$w_i = \begin{cases} 4/9, & i = 0 \\ 1/9, & i = 1,\ 3,\ 5,\ 7 \\ 1/36, & i = 2,\ 4,\ 6,\ 8 \end{cases}. \tag{5}$$

After evolution, the macroscopic variables density and velocity are calculated by

$$\rho = \sum_i f_i, \tag{6}$$

$$\rho \boldsymbol{u} = \sum_i f_i \boldsymbol{e_i} = \sum_i f_i^{\mathrm{eq}} \boldsymbol{e_i}, \tag{7}$$

and the pressure (p) is given by

$$p = \frac{1}{3}\rho c^2. \tag{8}$$

2.2 | Original immersed moving boundary method

A brief introduction of the original IMB method[19] is presented here, which includes two basic aspects. First, the no-slip boundary condition should be satisfied on the solid surface. Second, the hydrodynamic force imposed on the particle needs be calculated to update the particle dynamics. In IMB the fluid exists in both inside (internal fluid) and outside (external fluid) of the solid particle. Internal fluid moves rigidly with the solid particle to ensure the no-slip boundary condition, which is achieved by introducing a fluid-solid interaction term Ω_i^s in the standard LB equation (Equation (1))

$$f_i(\boldsymbol{x} + \boldsymbol{e_i}\delta_t, t + \delta_t) = f_i(\boldsymbol{x}, t) + (1 - B)\left\{-\frac{1}{\tau}[f_i(\boldsymbol{x}, t) - f_i^{\mathrm{eq}}(\rho, \boldsymbol{u})]\right\} + B\Omega_i^s. \tag{9}$$

The fluid-solid interaction term Ω_i^s is derived by the bounce-back for the nonequilibrium part of particle distribution f_i.[9]

$$\Omega_i^s = [f_{-i}(\boldsymbol{x}, t) - f_{-i}^{\mathrm{eq}}(\rho, \boldsymbol{u})] - [f_i(\boldsymbol{x}, t) - f_i^{\mathrm{eq}}(\rho, V_p)], \tag{10}$$

where V_p is the particle velocity at position $\boldsymbol{x}$. In Equation (9), B is a weight function depending on the volume fraction γ occupied by solid in each LBM cell

$$B = \frac{\gamma(\tau - 0.5)}{(1 - \gamma) + (\tau - 0.5)}. \tag{11}$$

$B = 0$ when $\gamma = 0$, and $B = 1$ when $\gamma = 1$. Thus, Equation (9) degenerates into the standard LB equation (Equation (1)) and the bounce-back rule for $\gamma = 0$ and 1, respectively. In this work, the cell decomposition method[10] is used to calculate the volume fraction γ in each LBM cell, whose detail implementation is presented in Appendix A.

To derive the hydrodynamic force imposed on the solid particle, Equation (9) is rewritten as the standard form of LB equation (Equation (1))

$$f_i(\boldsymbol{x} + \boldsymbol{e_i}\delta_t, t + \delta_t) = f_i(\boldsymbol{x}, t) - \frac{1}{\tau}[f_i(\boldsymbol{x}, t) - f_i^{\mathrm{eq}}(\rho, \boldsymbol{u})] + \frac{B}{\delta_t}\left\{\frac{1}{\tau}[f_i(\boldsymbol{x}, t) - f_i^{\mathrm{eq}}(\rho, \boldsymbol{u})] + \Omega_i^s\right\}\delta_t. \tag{12}$$

Compared with Equation (1), an external force at discrete direction $\boldsymbol{e_i}$ is introduced in IMB to enforce the no-slip boundary condition, whose magnitude is given by

$$\frac{B}{\delta_t}\left\{\frac{1}{\tau}[f_i(\boldsymbol{x}, t) - f_i^{\mathrm{eq}}(\rho, \boldsymbol{u})] + \Omega_i^s\right\}. \tag{13}$$

For LBM cell inside the particle, the total external force is sum of Equation (13) at all discrete direction $\boldsymbol{e_i}$

$$\sum_i \frac{\delta_x^3 B}{\delta_t}\left\{\frac{1}{\tau}[f_i(\boldsymbol{x}, t) - f_i^{\mathrm{eq}}(\rho, \boldsymbol{u})] + \Omega_i^s\right\}\boldsymbol{e_i}. \tag{14}$$

Based on Equation (7), $\sum_i \frac{1}{\tau}[f_i(\boldsymbol{x}, t) - f_i^{\mathrm{eq}}(\rho, \boldsymbol{u})]\boldsymbol{e_i} = 0$, so Equation (14) is rewritten as

$$\sum_i \frac{\delta_x^3 B}{\delta_t}\Omega_i^s \boldsymbol{e_i}. \tag{15}$$

Thus, the original IMB method can be regarded as a special scheme to deal with the local body force. The total hydrodynamic force imposed on solid particle is calculated by summing the external force in n cells covered by it, while the direction is opposite

$$\boldsymbol{F} = -\sum_n \left(\sum_i \frac{\delta_x^3 B_n}{\delta_t}\Omega_i^s \boldsymbol{e_i}\right), \tag{16}$$

where B_n is the weighting function in nth LBM cell inside the solid particle. The torque is calculated similarly by

$$\boldsymbol{T} = -\sum_n \left[\sum_i \frac{\delta_x^3 B_n}{\delta_t}\Omega_i^s \boldsymbol{e_i}(\boldsymbol{x_n} - \boldsymbol{x}_{\mathrm{cm}})\right], \tag{17}$$

where $\boldsymbol{x_n}$ is the nth cell position, and $\boldsymbol{x}_{\mathrm{cm}}$ is the mass center of the solid particle.

3 | IMPROVED IMMERSED MOVING BOUNDARY METHOD

In IMB, the no-slip boundary condition can be satisfied well, and its accuracy and convergence characteristics have been discussed in Reference [10]. However, the hydrodynamic force calculated by IMB is still not sufficiently accurate especially when the particle velocity is relatively high.[11] Inspired by the internal fluid correction for traditional immersed boundary method (IBM)[49,50] (a totally different approach dealing with the moving boundary condition from IMB), we find that the origin of inaccurate hydrodynamic force in IMB also comes from the internal fluid effect.

In IMB, the internal fluid moves with the solid particle, but in the real case the solid particle is "solid and dry" and only the external fluid exists. Thus, it is necessary to explore how the internal fluid affects the hydrodynamic force calculation in IMB. In order to answer this question, a strict mathematic derivation of the hydrodynamic force in the framework of IMB method is given as follows.

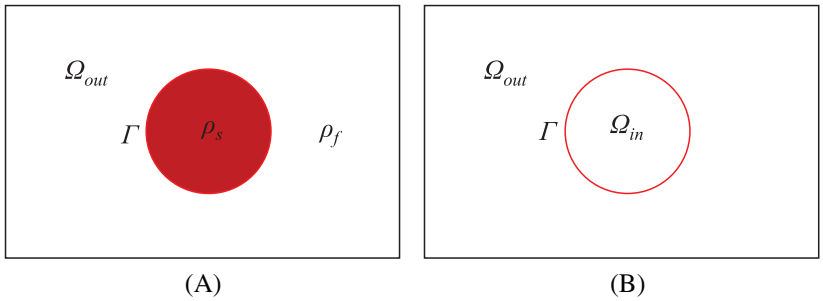

FIGURE 1 Diagram for particle suspension in real case and in the framework of IMB method [Colour figure can be viewed at wileyonlinelibrary.com]

3.1 | Mathematical derivation for hydrodynamic force in IMB

Inspired by the previous research of IBM,[49-51] we consider a single particle suspended in fluid. A rigid solid particle with density ρ_s is immersed in the fluid with density ρ_f and the domain Ω (see Figure 1A). In the framework of IMB method, the domain Ω includes two parts, internal fluid Ω_{in} and external fluid Ω_{out}, Γ is the solid boundary (see Figure 1B).

First, consider the "solid and dry" particle in Figure 1A. Its motion is governed by the Newton-Euler equation as

$$m_s \frac{du_s}{dt} = \oint_\Gamma \boldsymbol{\tau} \cdot \boldsymbol{n} ds + \boldsymbol{F}_{\text{external}}, \tag{18}$$

$$I_s \frac{d\boldsymbol{\varpi}_s}{dt} + \varpi_s \times [I \cdot \boldsymbol{\varpi}_s] = \oint_\Gamma \boldsymbol{\tau} \cdot \boldsymbol{n} \times (\boldsymbol{x} - \boldsymbol{x}_{\text{cm}}) ds + \boldsymbol{T}_{\text{external}}, \tag{19}$$

where the first terms on the right hand are hydrodynamic force and torque, respectively, and the second terms are external force (such as gravity) and torque imposed on the solid particle. In IMB, fluid exists inside and outside the solid particle (see Figure 1B). When the internal fluid Ω_{in} is considered as a whole, its motion is governed by

$$\frac{d}{dt} \int_{\Omega_{\text{in}}} \rho_f \boldsymbol{u_f} dV = \oint_\Gamma \boldsymbol{\tau}^* \cdot \boldsymbol{n} ds + \rho_f \int_{\Omega_{\text{in}}} \boldsymbol{f} dV, \tag{20}$$

$$\frac{d}{dt} \int_{\Omega_{\text{in}}} I_f^* \boldsymbol{\varpi_f} dV = \oint_\Gamma \boldsymbol{\tau}^* \cdot \boldsymbol{n} \times (\boldsymbol{x} - \boldsymbol{x}_{\text{cm}}) ds + \rho_f \int_{\Omega_{\text{in}}} \boldsymbol{f} \times (\boldsymbol{x} - \boldsymbol{x}_{\text{cm}}) dV, \tag{21}$$

where the first terms on right hand are force and torque imposed on the boundary of internal fluid Γ by external fluid Ω_{out}, and the second terms are force and torque caused by the body force of internal fluid. Due to the no-slip boundary condition, τ^* in Equations (20) and (21) is equal to τ in Equations (18) and (19). Substituting $\oint_\Gamma \boldsymbol{\tau} \cdot \boldsymbol{n} ds$ and $\oint_\Gamma \boldsymbol{\tau} \cdot \boldsymbol{n} \times (\boldsymbol{x} - \boldsymbol{x}_{\text{cm}}) ds$ by $\oint_\Gamma \boldsymbol{\tau}^* \cdot \boldsymbol{n} ds$ and $\oint_\Gamma \boldsymbol{\tau}^* \cdot \boldsymbol{n} \times (\boldsymbol{x} - \boldsymbol{x}_{\text{cm}}) ds$, respectively, Equations (18) and (19) are rewritten as

$$m_s \frac{du_s}{dt} = \frac{d}{dt} \int_{\Omega_{\text{in}}} \rho_f \boldsymbol{u_f} dV - \rho_f \int_{\Omega_{\text{in}}} \boldsymbol{f} dV + \boldsymbol{F}_{\text{external}}, \tag{22}$$

$$I_s \frac{d\boldsymbol{\varpi}_s}{dt} + \varpi_s \times [I_s \cdot \boldsymbol{\varpi}_s] = \frac{d}{dt} \int_{\Omega_{in}} I_f^* \boldsymbol{\varpi_f} dV - \rho_f \int_{\Omega_{\text{in}}} \boldsymbol{f} \times (\boldsymbol{x} - \boldsymbol{x}_{\text{cm}}) dV + \boldsymbol{T}_{\text{external}}. \tag{23}$$

Here is the strict mathematic expression (Equations (22) and (23)) for hydrodynamic force and torque in IMB, and the first terms on the right hand are the internal fluid effect.

In IMB, the body force of the internal fluid has been derived as $\sum_i \frac{\delta_x^3 B}{\delta_t} \Omega_i^s \boldsymbol{e_i}$ (see Equation (14)), and Equations (22) and (23) are expressed as

$$m_s \frac{du_s}{dt} = \frac{d}{dt} \int_{\Omega_{in}} \rho_f \boldsymbol{u_f} dV - \sum_n \sum_i \frac{\delta_x^3 B_n}{\delta_t} \Omega_i^s \boldsymbol{e_i} + \boldsymbol{F}_{\text{external}}, \tag{24}$$

$$I_s\frac{d\boldsymbol{\varpi}_s}{dt}+\boldsymbol{\varpi}_s\times[I_s\cdot\boldsymbol{\varpi}_s]=\frac{d}{dt}\int_{\Omega_{in}}I_f^*\boldsymbol{\varpi_f}dV-\sum_n\left[\sum_i\frac{\delta_x^3B_n}{\delta_t}\Omega_i^s\boldsymbol{e_i}(\boldsymbol{x_n}-\boldsymbol{x_{cm}})\right]+\boldsymbol{T}_{\text{external}},\tag{25}$$

where the first two terms on the right hand are the hydrodynamic force and torque, respectively, and the third terms are the external force (such as gravity) and torque imposed on solid. However, in the original IMB method, the first terms (internal fluid effect) are ignored. This is why the original IMB method cannot give the hydrodynamic force accurately.

In order to obtain the numerical expression of Equations (24) and (25), different schemes dealing with the internal fluid effect (first term on right hand of Equations (24) and (25)) have been introduced.[49]

3.2 | Internal fluid effect

The first scheme has no internal fluid effect, which implies the following assumptions

$$\frac{d}{dt}\int_{\Omega_{in}}\rho_f\boldsymbol{u_f}dV=0,\tag{26}$$

$$\frac{d}{dt}\int_{\Omega_{in}}I_f\boldsymbol{\varpi_f}dV=0.\tag{27}$$

With these assumptions, the internal fluid effect vanishes, and the hydrodynamic force calculated by Equations (16) and (17) is the same as that by the original IMB method. Clearly, these assumptions (Equations (26) and (27)) are only valid for the constant internal fluid velocity cases. This is why the original IMB method gave correct results for the fixed particle cases[9] where the internal fluid velocity was always equal to zero. However, in most cases, the particle velocity varies with time, and the correction for the internal fluid effect has to be considered.

3.2.1 | Implicit rigid motion approximation

A simple way to consider the internal fluid effect is to assume the internal fluid moves rigidly with the solid particle as follows

$$\frac{d}{dt}\int_{\Omega_{in}}\rho_f\boldsymbol{u_f}dV=\rho_fV\frac{d\boldsymbol{u_f}}{dt}=\rho_fV\frac{d\boldsymbol{u_s}}{dt},\tag{28}$$

$$\frac{d}{dt}\int_{\Omega_{in}}I_f^*\boldsymbol{\varpi_f}dV=I_f\frac{d\boldsymbol{\varpi_f}}{dt}=I_f\frac{d\boldsymbol{\varpi_s}}{dt}.\tag{29}$$

As a result, the governing equations (Equations (24) and (25)) are rewritten as

$$V(\rho_s-\rho_f)\frac{du_s}{dt}=-\sum_n\sum_i\frac{\delta_x^3B_n}{\delta_t}\Omega_i^s\boldsymbol{e_i}+\boldsymbol{F}_{\text{external}},\tag{30}$$

$$(I_s-I_f)\frac{d\boldsymbol{\varpi}_s}{dt}+\boldsymbol{\varpi}_s\times[I_s\cdot\boldsymbol{\varpi}_s]=-\sum_n\left[\sum_i\frac{\delta_x^3B_n}{\delta_t}\Omega_i^s\boldsymbol{e_i}(\boldsymbol{x_n}-\boldsymbol{x}_{\text{cm}})\right]+\boldsymbol{T}_{\text{extrenal}}.\tag{31}$$

In this scheme the internal fluid effect is considered implicitly by introducing an equivalent mass $V(\rho_{\text{s}}-\rho_{\text{f}})$ and moment of inertia $(I_{\text{s}}-I_{\text{f}})$, which is similar with the treatment in Ladd's shell model.[1,2] However, the solid-fluid density ratio is constrained in this scheme to obtain a stable update of particle position.[52-54]

$$\frac{\rho_{\text{s}}}{\rho_{\text{f}}}>1+\frac{10}{r},\tag{32}$$

where r is the radius of the sphere particle and when the solid-fluid density ratio is close to 1, stable results cannot be available.

3.2.2 | Explicit rigid motion approximation

In order to overcome the limitation of solid-fluid density ratio in implicit rigid motion approximation, an explicit scheme is considered here.[49]

$$\frac{d}{dt}\int_{\Omega_{\text{in}}}\rho_f \boldsymbol{u_f} dV = \rho_f V\frac{d\boldsymbol{u_f}}{dt} = \rho_f V\frac{d\boldsymbol{u_s}}{dt} \approx \rho_f V\frac{\boldsymbol{u_s}(t)-\boldsymbol{u_s}(t-\delta_t)}{\delta_t}, \tag{33}$$

$$\frac{d}{dt}\int_{\Omega_{in}} I_f^* \boldsymbol{\varpi_f} dV = I_f\frac{d\boldsymbol{\varpi_f}}{dt} = I_f\frac{d\boldsymbol{\varpi_s}}{dt} \approx I_f\frac{\boldsymbol{\varpi_s}(t)-\boldsymbol{\varpi_s}(t-\delta_t)}{\delta_t}. \tag{34}$$

When $t = 0$, $\boldsymbol{u_s}(-\delta_t) = \boldsymbol{u_s}(0)$, and $\boldsymbol{\varpi_s}(-\delta_t) = \boldsymbol{\varpi_s}(0)$. Substitution of Equations (33) and (34) into Equations (24) and (25) leads to a numerical scheme considering the internal fluid correction for hydrodynamic force:

$$m_s\frac{du_s}{dt} = \rho_f V\frac{\boldsymbol{u_s}(t)-\boldsymbol{u_s}(t-\delta_t)}{\delta_t} - \sum_n\sum_i \frac{\delta_x^3 B_n}{\delta_t}\Omega_i^s \boldsymbol{e_i} + \boldsymbol{F}_{\text{extrenal}}, \tag{35}$$

$$I_s\frac{d\boldsymbol{\varpi}_s}{dt} + \varpi_s \times [I_s \cdot \boldsymbol{\varpi}_s] = I_f\frac{\boldsymbol{\varpi_s}(t)-\boldsymbol{\varpi_s}(t-\delta_t)}{\delta_t} - \sum_n\left[\sum_i \frac{\delta_x^3 B_n}{\delta_t}\Omega_i^s \boldsymbol{e_i}(\boldsymbol{x_n}-\boldsymbol{x}_{\text{cm}})\right] + \boldsymbol{T}_{\text{external}}, \tag{36}$$

where V is the volume of solid particle, $\boldsymbol{F}_{\text{external}}$ and $\boldsymbol{T}_{\text{external}}$ is the external force and torque imposed on solid, respectively, I_{f} is the moment of inertia for internal fluid calculated by $I_{\text{f}} = \frac{\rho_{\text{f}}}{\rho_{\text{s}}} I_{\text{s}}$. Equations (35) and (36) are the final expressions of hydrodynamic force and torque in the current improved IMB method, where the first term on right hand is the internal fluid correction. In contrast to Equations (30) and (31), the current model applies an explicit scheme to approximate the rigid motion of the internal fluid, so it has no limitation on the solid-fluid density ratio.[49]

4 | VALIDATIONS OF IMPROVED IMB METHOD

4.1 | No-slip boundary validation

The no-slip condition is tested by simulating the fluid flow through a fixed particle. The simulation domain is a channel with height $H = 0.004$ m and length $L = 0.01$ m. A fixed sphere with radius $r = 0.001$ is initially placed at the position (0.005 m, 0.002 m). A pressure difference (ΔP) is applied along the channel to drive the fluid flow. In order to test the accuracy of current model, three space steps ($dx = 2.0 \times 10^{-5}$ m, 4.0×10^{-5} m, and 8.0×10^{-5} m) are considered. At the equilibrium state, dimensionless velocity distribution along y direction at $x = 0.005$ m is plotted in Figure 2, which is normalized by $\frac{H^2\Delta P}{8\mu L}$. It can be seen that no-slip condition is perfectly satisfied at the particle surface and the results are mesh independent. The fluid velocity inside the particle is totally negligible, which is 3 order of magnitude lower than that outside the particle. To quantify the numerical error,ε_{err} is defined

$$\varepsilon_{\text{err}} = \frac{\sqrt{\sum_N (u^n - u^a)^2}}{N}, \tag{37}$$

where u^{n} is the numerical value of fluid velocity on particle surface, u^{a} is the analytical one ($u^a = 0$), and N is the total number of fluid grids on the particle surface. The dependence of numerical error on the grid number in the channel width is presented in Figure 3, which shows that the current model can preserve the first-order spatial accuracy.

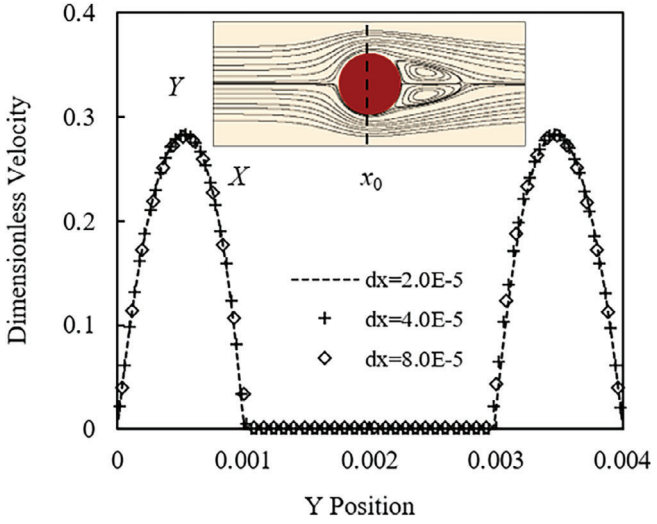

FIGURE 2 Dimensionless velocity distribution along the $x = x_0$ position, which shows that no-slip boundary can be greatly satisfied [Colour figure can be viewed at wileyonlinelibrary.com]

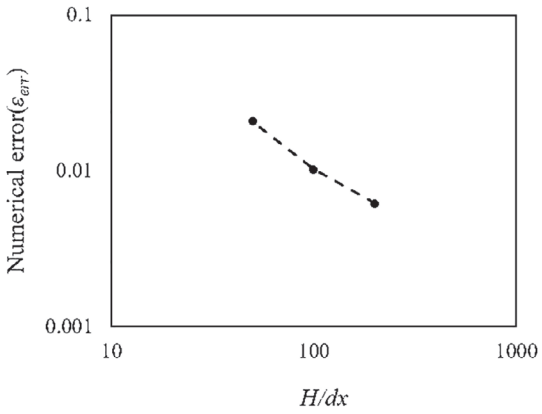

FIGURE 3 Error convergence rates of the velocity in the current simulation

4.2 | 2D elliptical particle sedimentation

To test the accuracy of the current model for the dynamic cases we consider a single elliptical particle sedimentation. We choose this case for benchmark comparison because (a) the direct simulations of a single elliptical particle sedimentation have been reported much in the previous studies[11,31,55-57] so that there is sufficient data available for the comparison and (b) the elliptical particle is more sensitive than the spherical one to the simulation error,[11] which is critical to evaluate new models.

The geometry of this case is shown in Figure 4, where a and b are the length of the semimajor and semiminor axis of the elliptical particle. The simulation domain is a closed channel with width L and height $30\,L$. Such a long channel is chosen to avoid the end effects from the top and bottom boundaries on the simulation results. The angle between the semimajor axis and y-axis at the negative direction is θ. Initially, the particle velocity is set at zero, and its motion in fluid is driven by the gravity along the x-axis in the positive direction. The parameters in this work are listed in Table 1 that are same as those in.[11] Bounce-back rule is applied on the left and right walls, and the fluid velocity on the top and bottom boundaries is set to zero. The elliptical particle is initially placed at the position (1.2 cm, 0.2 cm) with $\theta = 3\pi/4$. Reynolds number is calculated by the terminal velocity of the particle

$$\mathrm{Re} = \frac{u_s a}{\nu}, \tag{38}$$

where $u_s$is the particle terminal velocity.

In this case the Reynolds number is equal to 6.6. Since the direct simulation by FEM has been validated and usually regarded as the benchmark, the data in Reference [55] are used to evaluate new models for this problem. The comparisons are shown in Figures 5 and 6.

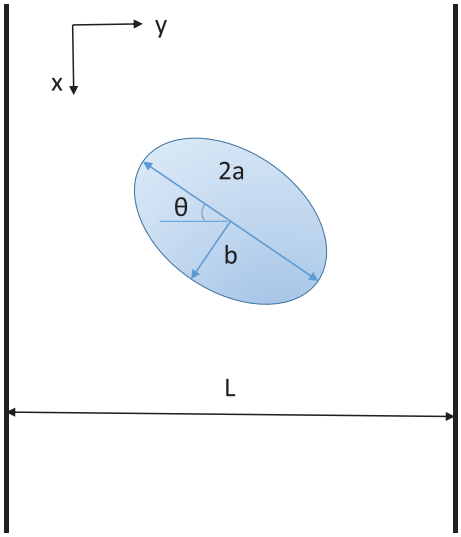

FIGURE 4 Geometry for the benchmark case, where L is the channel width, a and b are the length of semimajor and semiminor axis of the elliptical particle, respectively. Parameter θ is the angle between semimajor axis and y-axis at the negative direction. The elliptical particle settles in Newtonian fluid owing to the gravity [Colour figure can be viewed at wileyonlinelibrary.com]

TABLE 1 Parameters for current simulation in physical and lattice units

Parameter	Physical units	Lattice units
Semimajor a	0.05 cm	13
Semiminor b	0.025 cm	6.5
Channel width L	0.4 cm	104
Gravity G	9.8 m/s^2	6.20×10^{-4}
Viscosity ν	1.0×10^{-6} m^2/s	0.033
Fluid density ρ_f	1000 kg/m^3	1
Fluid density ρ_s	1100 kg/m^3	1.1

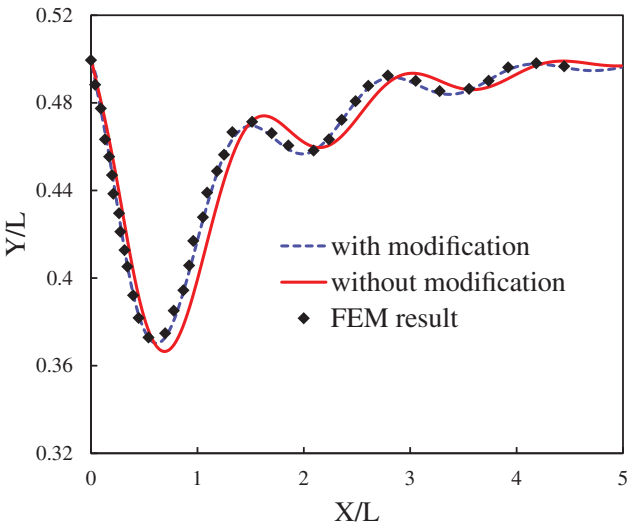

FIGURE 5 Comparison of particle trajectories for $Re = 6.6$ case. The black dot line is particle trajectories obtained by FEM,[55] which is used to evaluate other two methods. The red line is the result obtained by the previous IMB method, which deviates from the FEM result. The blue lines are the results considering the internal fluid correction, which agree well with that by FEM [Colour figure can be viewed at wileyonlinelibrary.com]

Figure 5 shows the comparison of the particle trajectories. The previous IMB method (see red one in Figure 5) deviates significantly from FEM data, which has been presented in the previous study similarly.[11] After considering the internal fluid correction by the explicit rigid motion approximation (Equations (35) and (36)), the particle trajectories agree well with that by FEM (see blue dot line in Figure 5). The current model can efficiently and accurately calculate the hydrodynamic force and torque. The particle orientation evolution in Figure 6 shows again that the current model agrees with the FEM results better.

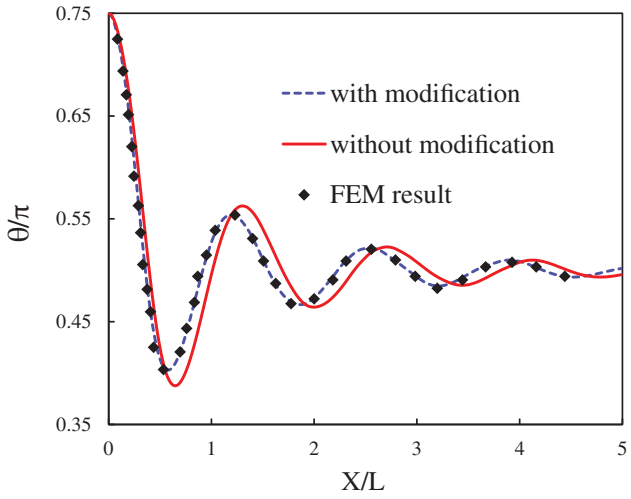

FIGURE 6 Comparison of particle orientation for $Re = 6.6$ case. The black dot line is the particle orientation obtained by FEM,[55] which is used to validate other two models. The red one is the result obtained by the previous IMB method, which deviates from the FEM result. The blue dot line is the result using the current improved model with the internal fluid correction, and a better agreement with the FEM result is obtained [Colour figure can be viewed at wileyonlinelibrary.com]

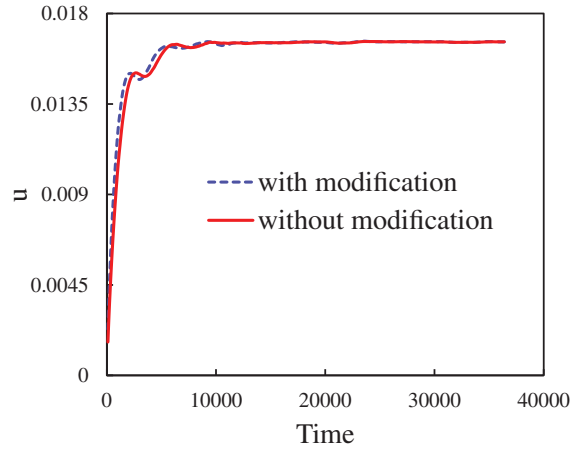

FIGURE 7 Comparison of translational velocity obtained by different methods for $Re = 6.6$ case. The red line is the particle translational velocity using the previous IMB method, and the blue dot one is the result obtained by the current improved model [Colour figure can be viewed at wileyonlinelibrary.com]

Figures 7 and 8 are the comparison of the translational and angular velocity obtained by the previous IMB method and the current improved one. For translational velocity, there is no significant difference between the previous method and the current one especially at the steady state (see Figure 7). However, the angular velocity obtained by the previous IMB deviates remarkably from that by the improved model (see Figure 8). Thus, the internal fluid has a more significant influence on the angular velocity than the translational velocity. In addition, when the steady state is obtained, the difference between these two models vanishes. Indeed, the internal fluid effect is caused by the inertial force of the internal fluid (see the first term on right hand of Equations (24) and (25)), so it vanishes when the steady state is obtained. Thus, the internal fluid in the original IMB affects the unsteady process yet has no influence on the terminal steady quantity. For this reason, the previous IMB cannot give the accurate particle trajectories and orientation in current simulations, but the terminal particle velocity is still correct. If we focus on the unsteady process of the solid-fluid coupling problem, the internal fluid correction has to be considered very carefully.

Smooth hydrodynamic force calculation is an important advantage of the original IMB method. Figure 9 shows the comparison of the hydrodynamic force obtained by different methods. Chen's results are from the corrected momentum exchange method,[11] which was the smoothest hydrodynamic force in all the momentum exchange based models they tested. Force fluctuation in the current model is smaller than that in Chen's midway bounce-back method and at nearly the same level as that in Chen's curved boundary bounce-back method. However, in curved boundary method interpolations and extrapolations are needed to determine the exact position of the solid particle. Thus, the advantage of smooth force calculation in the original IMB method is inherited by the current improved one. In addition, the extra computational cost in the current model is negligible, because the additional terms in Equations (35) and (36) are already obtained in the particle dynamics calculation procedure. In previous IMB, 10 000 steps need 610.8 seconds, and in

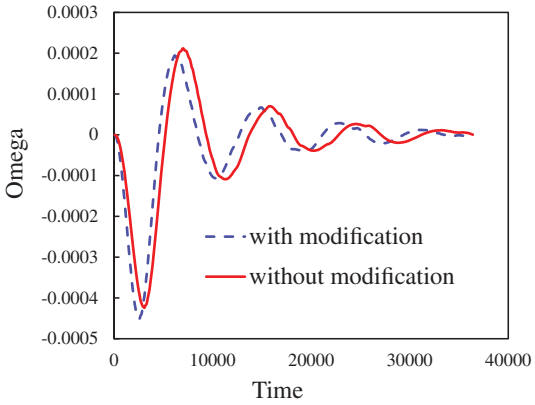

FIGURE 8 Comparison of angular velocity obtained by different methods for $Re = 6.6$ case. The red line is the particle angular velocity obtained by the previous IMB method, and the blue dot one is the result obtained by the current improved model [Colour figure can be viewed at wileyonlinelibrary.com]

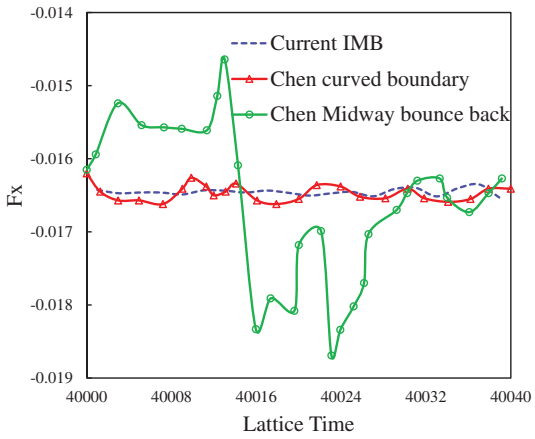

FIGURE 9 Comparison of hydrodynamic force obtained by different methods for $Re = 6.6$ case. The purple dot line is the hydrodynamic force obtained by the current improved model. The data in green and red lines are from,[11] and in that article Chen et al proposed a corrected momentum exchange method to reduce force fluctuation, where midway bounce back means the boundary of the solid particle is zigzag, and in curved boundary interpolation is applied to determine the exact position of the solid particle [Colour figure can be viewed at wileyonlinelibrary.com]

current model, the same process needs 613.7 seconds. However, current model cannot be expanded to two phase fluid solid coupled system, but momentum exchange based models has been used to simulate the particle motion in two phase fluids system.[58]

As mentioned above, the internal fluid effect is caused by the inertial force of the internal fluid that is proportional to the inertial force of the solid particle. Thus, the numerical error in the original IMB method depends on the inertial force of the solid particle. This is why the original IMB method works in some cases, but fails in others. For example, if a lower Reynolds number case is considered by decreasing the gravity imposed on the elliptical particle, the inertial force of the solid particle will decrease during the sedimentation process. As a result, the error caused by the absence of internal fluid correction will also decrease. On the contrary, if we increase the gravity acceleration of the solid particle, the error will increase. Our simulation results also confirm this conclusion, which are presented as follows.

Simulation results for relatively low and high Reynolds number cases are presented in this part. In $Re = 0.31$ case, the channel width (L) and length is equal to 100 and 3000, respectively. Initially, the elliptical particle is placed at the position of (3 L, 0.5 L) with $\theta = 45^o$. Parameter $a = 1.5b = 10$, gravity acceleration G = 1.355e-4, and solid-fluid density ratio is 1.0015. In LBM implementation, the dimensionless relaxation time $\tau = 0.6$. The particle trajectories and orientation are presented in Figure 10, where FEM results are obtained from.[59] When Reynolds number is relatively low ($Re = 0.31$), the inertia force of the solid particle is small. As a result, the numerical deviation when using the original IMB method is small.

In $Re = 11$ case, the physical model is same as that in $Re = 6.6$ case. For obtaining a relatively high Re, solid-fluid density ratio is raised to 3, and fluid viscosity is equal to 3.0×10^{-6} m^2/s. Channel width L is 208 in the lattice unit. Figure 11 shows the particle trajectories and orientation in $Re = 11$ case. Because FEM data are not available in this case, the LBM results in Reference [11] are used for the comparison. Current results agree well that in,[11] but the deviation is observed when using the original IMB method. Thus, the internal fluid in IMB method has a more significant effect in cases with higher Reynolds number.

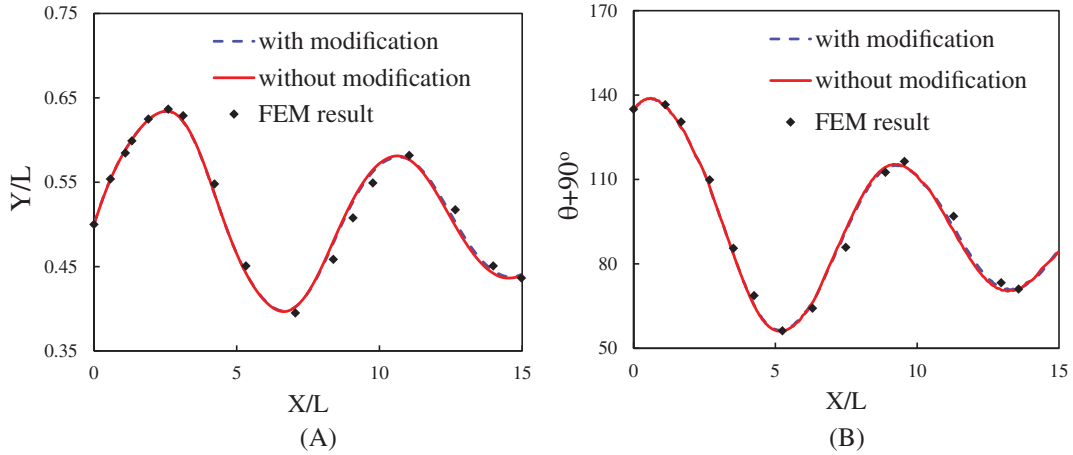

FIGURE 10 Comparison of the particle trajectories and orientation for $Re = 0.31$ case. The black dot line is the result obtained by FEM.[59] The red one is obtained by the previous IMB method. The blue dot line is the result by the current improved IMB method [Colour figure can be viewed at wileyonlinelibrary.com]

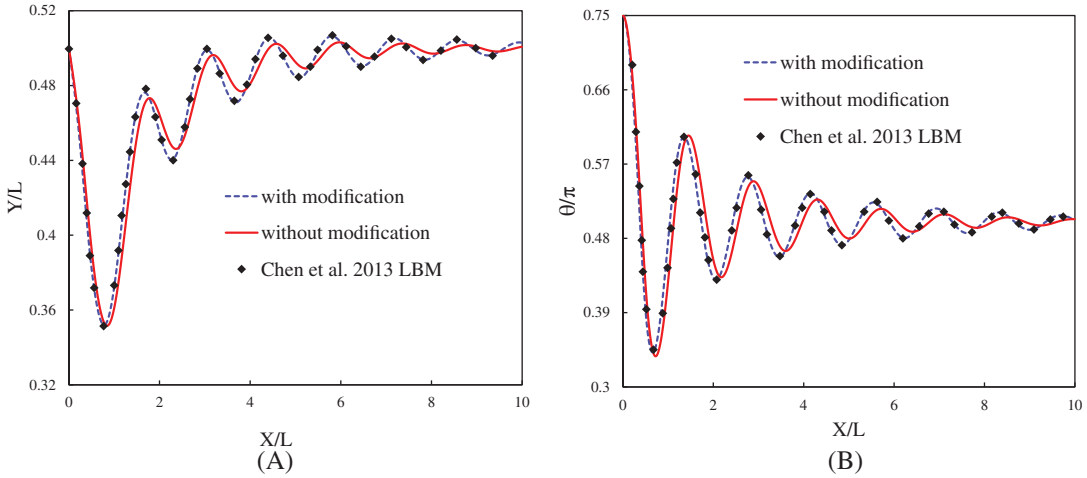

FIGURE 11 Comparison of particle trajectories and orientation for $Re = 11$ case. The black dot line is the result obtained by the momentum exchange methods proposed in.[11] The red one is obtained by the original IMB method, and the blue dot line is the result obtained by the current improved model [Colour figure can be viewed at wileyonlinelibrary.com]

4.3 | 3D sphere sedimentation

Current algorithm is very easy to be extended to 3D cases. In this subsection, a 3D sphere sedimentation in a closed cylinder with square cross-section is considered, which was also numerically or experimentally explored in the previous work.[49,60] In Reference [60], the sphere sedimentation is measured experimentally using cross correlation particle image velocimetry (PIV), and the data set consists of the velocity field of the fluid surrounding the settling sphere and the trajectory (ie, position as a function of time). The container dimensions in the experiment were chosen as $100 \times 100 \times 160$ mm, and a sphere with radius $r = 7.5$ mm and density $\rho_f = 1120\,\text{kg/m}^3$ is initially placed at the position (50, 50, 32.5) mm. The fluid is rest initially, whose density and viscosity are equal to $960\,\text{kg/m}^3$ and $0.058\,\text{N s/m}^2$ respectively. Due to the gravity acceleration ($9.8\,\text{m/s}^2$), the sphere settles in the x direction. The same process is simulated using current improved IMB and the original IMB. The domain is divided into $200 \times 200 \times 320$ lattice (see Figure 12). In LBM, the bounce-back rule is applied for the side walls, and the fluid velocity on top and bottom boundaries is set to zero.

Simulation results are shown in Figure 13, where the experimental results in Reference [60] are cited for the comparison. The current improved IMB method agrees reasonably with the experimental data, which shows the accuracy of

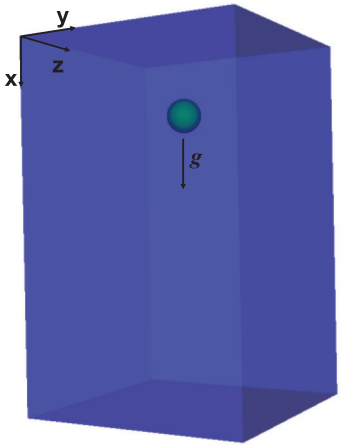

FIGURE 12 Diagram for the 3D sphere sedimentation in a closed box, where the gravity acceleration g is considered to drive the particle motion in the x direction [Colour figure can be viewed at wileyonlinelibrary.com]

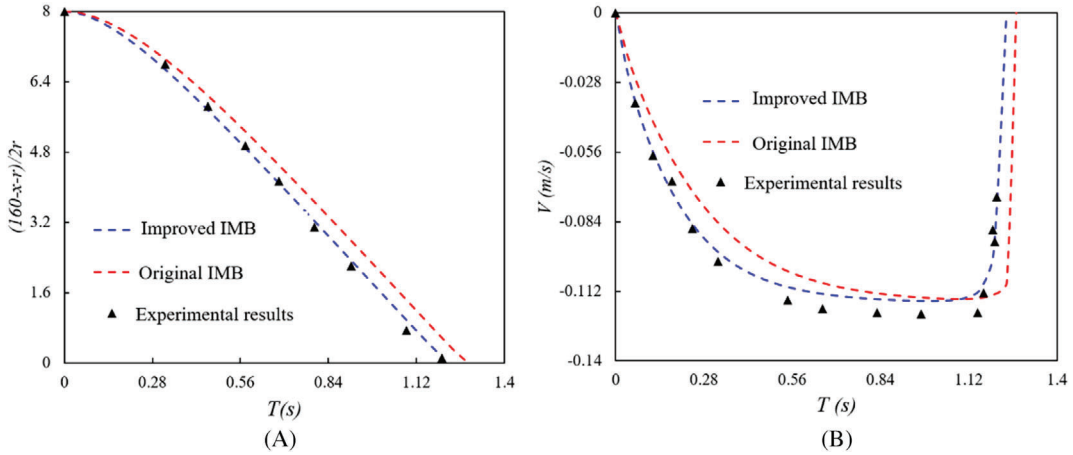

FIGURE 13 Comparison of, A, particle position and, B, velocity in x direction, where results obtained by the experiment[60] are cited to validate the current improved model in 3D cases. Results by the current improved model agree well with others, but deviations exist when using the previous IMB method

current model. However, a remarkable deviation exists for the original IMB method. Thus, to obtain the accurate hydrodynamic force, the internal fluid effect must be considered in the original IMB method for either 2D or 3D cases. The small discrepancy in the maximum velocity in Figure 13B is caused by the effective sphere radius in the simulation slightly different from the input radius. Other numerical methods also suffer from the same nonphysical dependency, which is not the main focus of this work, and more discussions about this problem can be found in References [2,49,60-62].

This process was also simulated in the previous work,[49] where the immersed boundary method (IBM) is applied to couple the fluid flow and the particle motion. The IBM is totally different from the current IMB model. In IMB model, the body force is applied on the whole fluid nodes inside the solid boundary, so that the internal fluid can move rigidly with the solid particle. Thus, unlike IBM, the IMB method does not suffer from the boundary penetration by the streamline just as presented in Figure 2.

5 | CONCLUSIONS

Accurate calculation of the interactive force between the solid and fluid is very important in studies of dense particle suspension in fluid. The previous immersed moving boundary assumes the fluid existing both inside and outside the solid particle, and ensure the no-slip boundary condition on the solid surfaces by introducing the external forces at the discrete

velocity direction for the internal fluid. The fake internal fluid significantly influences the hydrodynamic force calculation even though it does not affect the external fluid velocity and pressure distribution. We figure out the physical origin of the internal fluid effect in this work by the theoretical analysis, and propose a corrected immersed moving boundary by considering the internal fluid effect on the hydrodynamic force. This method is easy to implement and with negligible extra computational costs. In order to evaluate the new model, a series of cases are simulated, including a 2D elliptical particle and a 3D sphere sedimentation in the Newtonian fluid. The following conclusions are obtained:

1. The improved immersed moving boundary has been validated by comparisons with FEM and experimental data. The results show that the hydrodynamic force calculation is smooth that is prior to other momentum exchange based methods.
2. The fake fluid inside solid particle (internal fluid) has significant influences on the unsteady process (including particle trajectories and orientation), but little on the finial steady state (such as the terminal particle velocity). The present improved model works well to correct the errors from the internal fluid effects when the unsteady process is concerned.

ACKNOWLEDGEMENTS

This work is financially supported by the NSF of China Grant (No. 11761131012, U1837602), National Science and Technology Major Project on Oil and Gas (No. 2017ZX05013001) and Tsinghua University Initiative Scientific Research Program. The simulations are run on the "Explorer 100" cluster of Tsinghua National Laboratory for Information Science and Technology. There is no any conflict of interest in this work.

ORCID


Moran Wang https://orcid.org/0000-0002-0112-5150

REFERENCE

1. Ladd AJC. Numerical simulations of particulate suspensions via a discretized Boltzmann-equation 1 theoretical foundation. *J Fluid Mech*. 1994;271:285-310.
2. Ladd AJC. Numerical simulations of particulate suspensions via a discretized Boltzmann-equation 2 numerical results. *J Fluid Mech*. 1994;271:311-339.
3. Detournay E. Mechanics of hydraulic fractures. *Annu Rev Fluid Mech*. 2016;48:311-339.
4. Vardoulakis I, Stavropoulou M, Papanastasiou P. Hydro-mechanical aspects of the sand production problem. *Transp Porous Media*. 1996;22(2):225-244.
5. Ranjith PG, Perera MSA, Perera WKG, Choi SK, Yasar E. Sand production during the extrusion of hydrocarbons from geological formations: a review. *J Petrol Sci Eng*. 2014;124:72-82.
6. Wang S, Luo K, Yang S, Hu C, Fan J. Parallel LES-DEM simulation of dense flows in fluidized beds. *Appl Therm Eng*. 2017;111:1523-1535.
7. Chen ZQ, Xie C, Chen Y, Wang M. Bonding strength effects in hydro-mechanical coupling transport in granular porous media by pore-scale modeling. *Comput Secur*. 2016;4(1):18.
8. Feng YT, Han K, Owen DRJ. Coupled lattice Boltzmann method and discrete element modelling of particle transport in turbulent fluid flows: computational issues. *Int J Numer Methods Eng*. 2007;72(9):1111-1134.
9. Strack OE, Cook BK. Three-dimensional immersed boundary conditions for moving, solids in the lattice-Boltzmann method. *Int J Numer Methods Fluids*. 2007;55(2):103-125.
10. Owen DRJ, Leonardi CR, Feng YT. An efficient framework for fluid-structure interaction using the lattice Boltzmann method and immersed moving boundaries. *Int J Numer Methods Eng*. 2011;87(1–5):66-95.
11. Chen Y, Cai Q, Xia Z, Wang M, Chen S. Momentum-exchange method in lattice Boltzmann simulations of particle-fluid interactions. *Phys Rev E*. 2013;88(1):15.
12. Aidun CK, Lu YN, Ding EJ. Direct analysis of particulate suspensions with inertia using the discrete Boltzmann equation. *J Fluid Mech*. 1998;373:287-311.
13. Wen BH, Li H, Zhang C, Fang H. Lattice-type-dependent momentum-exchange method for moving boundaries. *Phys Rev E*. 2012;85(1):9.
14. Wang M, Feng YT, Wang CY. Coupled bonded particle and lattice Boltzmann method for modelling fluid-solid interaction. *Int J Numer Anal Methods Geomech*. 2016;40(10):1383-1401.
15. Filippova O, Hanel D. Lattice-Boltzmann simulation of gas-particle flow in filters. *Comput Fluids*. 1997;26(7):697-712.
16. Mei RW, Luo LS, Shyy W. An accurate curved boundary treatment in the lattice Boltzmann method. *J Comput Phys*. 1999;155(2):307-330.
17. Inamuro T, Maeba K, Ogino F. Flow between parallel walls containing the lines of neutrally buoyant circular cylinders. *Int J Multiphase Flow*. 2000;26(12):1981-2004.
18. Mei RW, Yu D, Shyy W, Luo LS. Force evaluation in the lattice Boltzmann method involving curved geometry. *Phys Rev E*. 2002;65(4):14.

19. Noble DR, Torczynski JR. A lattice-Boltzmann method for partially saturated computational cells. *Int J Modern Phys C*. 1998;9(8):1189-1201.
20. Galindo-Torres SA. A coupled discrete element lattice Boltzmann method for the simulation of fluid-solid interaction with particles of general shapes. *Comput Methods Appl Mech Eng*. 2013;265:107-119.
21. Chen Z, Yang Z, Wang M. Hydro-mechanical coupled mechanisms of hydraulic fracture propagation in rocks with cemented natural fractures. *J Petrol Sci Eng*. 2018;163:421-434.
22. Chen ZQ, Wang MR. Pore-scale modeling of hydromechanical coupled mechanics in hydrofracturing process. *J Geophys Res Solid Earth*. 2017;122(5):3410-3429.
23. Han Y, Cundall P. Verification of two-dimensional LBM-DEM coupling approach and its application in modeling episodic sand production in borehole. *Petroleum*. 2017;3(2):179-189.
24. Cook BK, Noble DR, Williams JR. A direct simulation method for particle-fluid systems. *Eng Comput*. 2004;21(2–4):151-168.
25. Feng YT, Han K, Owen DRJ. Combined three-dimensional lattice Boltzmann method and discrete element method for modelling fluid-particle interactions with experimental assessment. *Int J Numer Methods Eng*. 2010;81(2):229-245.
26. Galindo-Torres SA, Palma S, Quintero S, et al. An airblast hazard simulation engine for block caving sites. *Int J Rock Mech min Sci*. 2018;107:31-38.
27. Cui XL, Li J, Chan A, Chapman D. Coupled DEM-LBM simulation of internal fluidisation induced by a leaking pipe. *Powder Technol*. 2014;254:299-306.
28. Galindo-Torres SA, Scheuermann A, Mühlhaus HB, Williams DJ. A micro-mechanical approach for the study of contact erosion. *Acta Geotechnica*. 2015;10(3):357-368.
29. Han YH, Cundall PA. LBM-DEM modeling of fluid-solid interaction in porous media. *Int J Numer Anal Methods Geomech*. 2013;37(10):1391-1407.
30. Brumby PE, Sato T, Nagao J, Tenma N, Narita H. Coupled LBM-DEM micro-scale simulations of cohesive particle erosion due to shear flows. *Transp Porous Media*. 2015;109(1):43-60.
31. Peskin CS. Flow patterns around heart valves - numerical method. *J Comput Phys*. 1972;10(2):252.
32. Peskin CS. Numerical-analysis of blood-flow in heart. *J Comput Phys*. 1977;25(3):220-252.
33. Delouei AA, Nazari M, Kayhani MH, Succi S. Non-Newtonian unconfined flow and heat transfer over a heated cylinder using the direct-forcing immersed boundary-thermal lattice Boltzmann method. *Phys Rev E*. 2014;89(5):053312.
34. Delouei AA, Nazari M, Kayhani MH, Succi S. Immersed boundary - thermal lattice Boltzmann methods for non-Newtonian flows over a heated cylinder: a comparative study. *Commun Comput Phys*. 2015;18(2):489-515.
35. Delouei AA, Nazari M, Kayhani MH, Ahmadi G. A non-Newtonian direct numerical study for stationary and moving objects with various shapes: an immersed boundary - lattice Boltzmann approach. *J Aerosol Sci*. 2016;93:45-62.
36. Delouei AA, Nazari M, Kayhani MH, Kang SK, Succi S. Non-Newtonian particulate flow simulation: a direct-forcing immersed boundary-lattice Boltzmann approach. *Phys Stat Mech Appl*. 2016;447:1-20.
37. Thorimbert Y, Marson F, Parmigiani A, Chopard B, Lätt J. Lattice Boltzmann simulation of dense rigid spherical particle suspensions using immersed boundary method. *Comput Fluids*. 2018;166:286-294.
38. Wang ZY, Wang MR, Chen SY. Coupling of high Knudsen number and non-ideal gas effects in microporous media. *J Fluid Mech*. 2018;840:56-73.
39. Xie CY, Lei WH, Wang MR. Lattice Boltzmann model for three-phase viscoelastic fluid flow. *Phys Rev E*. 2018;97(2):11.
40. Xie CY, Lv WF, Wang MR. Shear-thinning or shear-thickening fluid for better EOR? - a direct pore-scale study. *J Petrol Sci Eng*. 2018;161:683-691.
41. He XT, Guo Y, Li M, Pan N, Wang M. Effective gas diffusion coefficient in fibrous materials by mesoscopic modeling. *Int J Heat Mass Transf*. 2017;107:736-746.
42. Chen Z, Jin X, Wang M. A new thermo-mechanical coupled DEM model with non-spherical grains for thermally induced damage of rocks. *J Mech Phys Solids*. 2018;116:54-69.
43. Delouei AA, Nazari M, Kayhani MH, Ahmadi G. Direct-forcing immersed boundary - non-Newtonian lattice Boltzmann method for transient non-isothermal sedimentation. *J Aerosol Sci*. 2017;104:106-122.
44. Afra B, Nazari M, Kayhani MH, Delouei AA, Ahmadi G. An immersed boundary-lattice Boltzmann method combined with a robust lattice spring model for solving flow-structure interaction problems. *App Math Model*. 2018;55:502-521.
45. Chen S, Doolen GD. Lattice Boltzmann method for fluid flows. *Annu Rev Fluid Mech*. 1998;30:329-364.
46. Wang M, Kang Q. Electrokinetic transport in microchannels with random roughness. *Anal Chem*. 2009;81(8):2953-2961.
47. Wang M, Wang J, Chen S. Roughness and cavitations effects on electro-osmotic flows in rough microchannels using the lattice Poisson-Boltzmann methods. *J Comput Phys*. 2007;226(1):836-851.
48. Guo Z, Shu C. *Lattice Boltzmann Method and its Applications in Engineering*. Vol 3. Singapore: World Scientific; 2013.
49. Suzuki K, Inamuro T. Effect of internal mass in the simulation of a moving body by the immersed boundary method. *Comput Fluids*. 2011;49(1):173-187.
50. Kempe T, Frohlich J. An improved immersed boundary method with direct forcing for the simulation of particle laden flows. *J Comput Phys*. 2012;231(9):3663-3684.
51. Uhlmann M. An immersed boundary method with direct forcing for the simulation of particulate flows. *J Comput Phys*. 2005;209(2):448-476.
52. Qi DW. Lattice-Boltzmann simulations of particles in non-zero-Reynolds-number flows. *J Fluid Mech*. 1999;385:41-62.

53. Ladd AJC, Verberg R. Lattice-Boltzmann simulations of particle-fluid suspensions. *J Stat Phys*. 2001;104(5–6):1191-1251.
54. Nguyen NQ, Ladd AJC. Lubrication corrections for lattice-Boltzmann simulations of particle suspensions. *Phys Rev E*. 2002;66(4):12.
55. Xia ZH, Connington KW, Rapaka S, Yue P, Feng JJ, Chen S. Flow patterns in the sedimentation of an elliptical particle. *J Fluid Mech*. 2009;625:249-272.
56. Tao S, Hu JJ, Guo ZL. An investigation on momentum exchange methods and refilling algorithms for lattice Boltzmann simulation of particulate flows. *Comput Fluids*. 2016;133:1-14.
57. Karimnejad S, Amiri Delouei A, Nazari M, Shahmardan MM, Mohamad AA. Sedimentation of elliptical particles using immersed boundary - lattice Boltzmann method: a complementary repulsive force model. *J Mol Liq*. 2018;262:180-193.
58. Chen Y, Kang Q, Cai Q, Wang M, Zhang D. Lattice Boltzmann simulation of particle motion in binary immiscible fluids. *Commun Comput Phys*. 2015;18(3):757-786.
59. Huang PY, Hu HH, Joseph DD. Direct simulation of the sedimentation of elliptic particles in oldroyd-B fluids. *J Fluid Mech*. 1998;362:297-325.
60. ten Cate A, Nieuwstad CH, Derksen JJ, van den Akker HEA. Particle imaging velocimetry experiments and lattice-Boltzmann simulations on a single sphere settling under gravity. *Phys Fluids*. 2002;14(11):4012-4025.
61. Rohde M, Derksen J, Van den Akker HJPRE. Volumetric method for calculating the flow around moving objects in lattice-Boltzmann schemes. *Phys Rev E*. 2002;65(5):056701.
62. He X, Zou Q, Luo LS, Dembo M. Analytic solutions of simple flows and analysis of nonslip boundary conditions for the lattice Boltzmann BGK model. *J Stat Phys*. 1997;87(1–2):115-136.

SUPPORTING INFORMATION

Additional supporting information may be found online in the Supporting Information section at the end of this article.

How to cite this article: Chen Z, Wang M. An improved immersed moving boundary for hydrodynamic force calculation in lattice Boltzmann method. *Int J Numer Methods Eng*. 2020;121:4493–4508. https://doi.org/10.1002/nme.6444

APPENDIX A. Volume fraction (γ) in Equation (11) is calculated by the cell decomposition method[10] (see Figure A1), where each LBM cell is decomposed into n^2 subcells with side length $\Delta x_{\mathrm{sub}} = \delta_x/n$. In current case, 10 × 10 subcells are used for each 2D LBM cell. Those n^2 subcells are checked one by one to obtain the total subcells inside the solid particle (n_{in}), and then volume fraction (γ) is given by

$$\gamma = \frac{n_{\mathrm{in}}}{n^2}. \tag{A1}$$

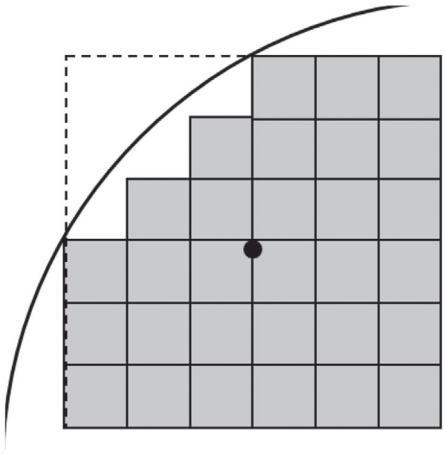

FIGURE A1 Diagram of decomposition method for volume fraction (γ) calculation, where each LBM cell is decomposed into n^2 subcells. The gray ones are subcells inside the solid boundary